Surface Science 603 (2009) 40–49

Contents lists available at ScienceDirect

Surface Science

journal homepage: www.elsevier.com/locate/susc

The adsorption of CO_2 and CO on Ca and CaO films studied with MIES, UPS and XPS

F. Voigts [a], F. Bebensee [b], S. Dahle [a], K. Volgmann [a], W. Maus-Friedrichs [a,*]

[a] Institut für Physik und Physikalische Technologien, Technische Universität Clausthal, Leibnizstrasse 4, 38678 Clausthal-Zellerfeld, Germany
[b] Lehrstuhl für Physikalische Chemie II, Universität Erlangen-Nürnberg, Egerlandstrasse 3, 91058 Erlangen, Germany

ARTICLE INFO

Article history:
Received 19 May 2008
Accepted for publication 14 October 2008
Available online 21 October 2008

Keywords:
Metastable induced electron spectroscopy
Photoelectron spectroscopy
Calcium
Calcium oxide
Carbon monoxide
Carbon dioxide
Calcium carbonate
Chemisorption

ABSTRACT

Metastable Induced Electron Spectroscopy (MIES), Ultraviolet Photoelectron Spectroscopy (UPS), and X-ray Photoelectron Spectroscopy (XPS) are employed to study the adsorption of CO_2 and CO on Ca and CaO films. Ca films are prepared by evaporation of Ca onto clean Si(100) substrates. CaO films are produced by Ca evaporation in an oxygen atmosphere at a substrate temperature of 670 K. CO_2 interaction with the Ca films is initiated by dissociation of the impinging molecules leading to the formation of Ca–O bonds. These Ca–O bonds are subsequently consumed in the formation of a closed $CaCO_3$ layer on top of the surface. CO interaction with the Ca surfaces also leads to the dissociation of the molecule and the formation of Ca–O bonds. We find evidence for the subsequent formation of CO_3^{2-} complexes on top of the surface. On CaO surfaces, both CO_2 and CO lead to the formation of a closed $CaCO_3$ top layer, though displaying very different reaction rates.

1. Introduction

The interaction between CO and CO_2 molecules and metals is of great interest in many respects: besides the more general interest in dissociation processes and their impact on the corrosion and passivation chemistry [1,2], the interaction of these gases with Ca has several other fields of use.

Alkaline earth titanates show a macroscopic change in electrical conductivity as a function of ambient oxygen partial pressure making especially $SrTiO_3$ useful in high temperature sensor applications [3]. In this context, the interaction between Sr and several gases has been studied [4], yet although Ca has been found to enhance the performance of $SrTiO_3$ sensors [5], few studies have been conducted focusing on the interaction between Ca and different gases, except for our recent study on the adsorption of O_2 and H_2O on Ca [6,7]. Furthermore, Ca is used as a promoter in catalytic reactions such as methane reforming with CO_2 [8]. A lot of studies deal with the effect of Ca on a (model) catalyst without investigating the interaction of Ca itself with different gases, although this might contribute considerably to the understanding of the role of Ca as a promoter in catalysis. Very recently, a detailed study of the adsorption of CO and CO_2 on CaO(100) appeared [9]. CaO shows catalytic activity, too, e.g. in the oxidation of lower alkanes using CO_2 as the oxidant. Such reactions are highly desirable, as low grade natural gas contains high quantities of CO_2, CH_4 and other lower alkanes, which can be converted to higher valued chemicals (C_2H_4 and C_2H_6) with simultaneously lowering the CO_2 emission using CaO based catalysts [10]. Furthermore, CaO is commonly used in desulfurization: Carnes and Klabunde found nanocrystalline CaO to be very efficient in the selective removal of highly toxic and corrosive H_2S from crude oil and natural gas [11]. Similarly, CaO based sorbents can be used for the removal of SO_2 from flue gases [12].

With the development of organic electronic devices [13] such as organic light emitting diodes (OLEDs), Ca has found yet another application as an electron injecting electrode owing to its low work function. Here, the interface of Ca with the polymers is of great importance, as it critically influences the device performance. Again, the knowledge about interactions taking place between Ca and different species may prove helpful in a more complete understanding of the underlying processes of the interaction between Ca and semiconducting polymers. Besides a number of XPS studies on the interaction between a semiconducting polymer and different metals, Zhu et al. have utilized adsorption microcalorimetry to study the interaction between Ca and polymethyl methacrylate [14], which was shown to be essentially the interaction of the Ca atoms with oxygen in the polymer. As polymers are not impermeable for gases, CO and CO_2 induced degradation processes probably occur and thus studying the interaction of those gases with Ca may be of value.

In this paper, we present Metastable Induced Electron Spectroscopy (MIES) and Ultraviolet Photoelectron Spectroscopy (UPS) data complemented by X-ray Photoelectron Spectroscopy (XPS) for the

* Corresponding author. Tel.: +49 5323 722310; fax: +49 5323 723600.
E-mail address: w.maus-friedrichs@pe.tu-clausthal.de (W. Maus-Friedrichs).

0039-6028/$ - see front matter © 2008 Elsevier B.V. All rights reserved.
doi:10.1016/j.susc.2008.10.016

adsorption of CO_2 and CO on Ca and CaO films under ultrahigh vacuum (UHV) conditions. This completes our previous study on the adsorption of H_2O and O_2 on Ca and CaO [6].

In a previous work we published very first results for the chemisorption of CO_2 on Ca and CaO surfaces [7]. It was found that CO_2 adsorbs dissociatively on Ca at low exposures forming Ca–O bonds. Subsequent CO_3^{2-} formation, via reaction of CO_2 with surface oxygen, is observed on top of the surfaces. Our recent examinations show however, that these experiments suffer from significant water impurities. This study avoids this problem and expands the object of investigation to carbon monoxide. Furthermore, detail XPS investigations were performed enhancing [7].

2. Experimental

An ultrahigh vacuum apparatus with a base pressure of 5×10^{-11} mbar, which has been described in detail previously [15], is used to carry out the spectroscopic measurements. All experiments were carried out at room temperature.

Electron spectroscopy is performed using a hemispherical analyzer (VSW HA100) in combination with a source for metastable helium atoms (mainly $He^* 2^3S$) and ultraviolet photons (HeI line). A commercial non-monochromatic X-ray source (Specs RQ20/38C) is utilized for XPS.

During XPS, X-ray photons hit the surface under an angle of 80° to the surface normal, illuminating a spot of several mm in diameter. For all measurements presented here, the Al Kα line with photon energy of 1486.7 eV is used. Electrons are recorded by the hemispherical analyzer with an energy resolution of 1.1 eV under an angle of 10° to the surface normal. All XPS spectra are displayed as a function of binding energy with respect to the Fermi level.

For quantitative XPS analysis, photoelectron peak areas are calculated via mathematical fitting with Gauss-type profiles using OriginPro 7G including the PFM fitting module, which uses Levenberg–Marquardt algorithms to achieve the best agreement possible between experimental data and fit. Peak widths (full width at half maximum, FWHM) and binding energy shifts from prelimary experiments on CaO and $CaCO_3$ are used as input parameters for the fits. The absolute values of the FWHMs depend on the resolution of the energy dispersive element used, while absolute binding energy values may be influenced by local charging of the surface. Photoelectric cross sections as calculated by Scofield [16] and inelastic mean free paths from the NIST database [17] as well as the energy dependent transmission function of our hemispherical analyzer are taken into account when calculating stoichiometry. Our experimental experience and the good reproducibility of the experiments allow us to estimate the typical deviation in our results to be certainly below 10%.

MIES and UPS are performed applying a cold cathode gas discharge via a two-stage pumping system. A time-of-flight technique is employed to separate electrons emitted by He^* (MIES) from those caused by HeI (UPS) interaction with the surface. The combined He^*/HeI beam strikes the sample surface under an angle of 45° to the surface normal and illuminates a spot of approximately 2 mm in diameter. The spectra are recorded simultaneously by the hemispherical analyzer with an energy resolution of 220 meV under normal emission within 150 s.

MIES is an extremely surface sensitive technique probing solely the outermost layer of the sample, because the He^* atoms interact with the surface typically 0.3–0.5 nm in front of it. This may occur via a number of different mechanisms depending on surface electronic structure and work function, as is described in detail elsewhere [18–20]. Only the processes relevant for the spectra presented here shall be discussed shortly.

During auger deexcitation (AD) an electron from the sample fills the 1s orbital of the impinging He^*. Simultaneously, the He 2s electron carrying the excess energy is emitted. The resulting spectra reflect the surface density of states (SDOS) directly. AD-MIES and UPS can be compared and allow a distinction between surface and bulk effects.

For low work functions below about 2.2 eV, the resonant transfer of an electron from the surface to the 2s orbital of the impinging He^* atom becomes sufficiently probable. This results in a He^{*-} ($1s^1 2s^2$) ion in front of the sample surface which decays via an autodetachment (AU) process into its ground state very quickly [21]. Hereby, one 2s electron undergoes a transition into the 1s level while the other 2s electron is emitted carrying the excess energy. This process produces a sharp structure near a kinetic energy of about 19 eV with a typical full width at half maximum (FWHM) of 0.7 eV.

All MIES and UPS spectra are displayed as a function of the electron binding energy with respect to the Fermi level. The surface WF can be determined from the high binding energy onset of the MIES or the UPS spectra with an accuracy of ±0.1 eV.

Calcium layers were prepared by evaporating calcium (Sigma–Aldrich, 99%) with a commercial UHV evaporator (Omicron EFM3) onto a Si(100) target. The Si target is cleaned by heating to approximately 1320 K prior to deposition. Calcium is subsequently offered at a rate of 0.85 nm min^{-1} for 300 s at room temperature. This procedure results in calcium layers of about 4.25 nm thickness as estimated from XPS measurements. In MIES and UPS, no signal due to the Si substrate can be detected for layers of this thickness. Structural information on these films have been presented in [7] by means of scanning tunneling microscopy (STM).

CaO layers were prepared by evaporation of Ca at a rate of 0.45 nm min^{-1} in an oxygen partial pressure of 6.7×10^{-7} mbar for 900 s at a target temperature of 670 K. Temperature and oxygen pressure are subsequently held for two minutes after stop of Ca evaporation. This procedure results in calcium oxide layers of about 6.75 nm thickness.

A XPS survey spectrum of a calcium oxide film is shown in Fig. 1. The spectrum was recorded for film thickness calculation using the attenuation of the Si 2p and Si 2s peaks; therefore, the oxide is intentionally about 50% thinner than the ones used for gas adsorption experiments. The stoichiometry as calculated from Ca 2p and O 1s peak areas amounts to 52% calcium and 48% oxygen, thus verifying the growth of an exactly stoichiometric oxide within the accuracy of our setup. This spectrum shows no and the lowermost MIES/UPS spectra of these films in Figs. 5 and 12

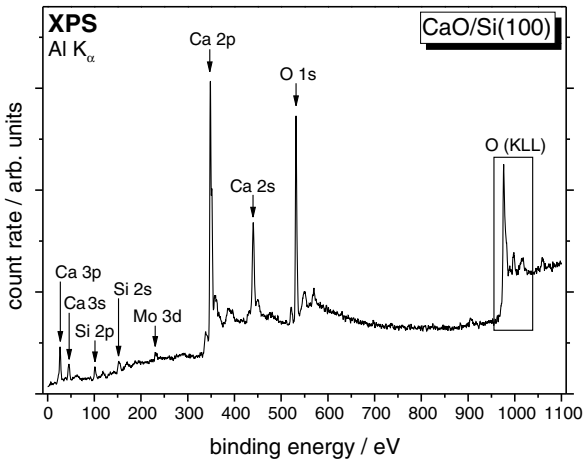

Fig. 1. XPS survey spectrum of a calcium oxide film.

only very slight contaminations of the oxide due to the presence of low amounts of water during evaporation. The small molybdenum content stems from the sample holder and does not indicate a contamination of the sample itself.

CO_2 (Linde Gas, 99.995%) and CO (Linde Gas, 99.97%) are offered via backfilling the chamber using a bakeable leak valve. The gas line is evacuated and can be heated in order to ensure cleanness. Additionally, a cold-trap is installed to minimize water contamination during gas dosage. A quadrupole mass spectrometer (Balzers QMS 112A) is used to monitor the partial pressure of the reactive gases simultaneously during all MIES and UPS measurements.

Additional XPS experiments (not shown here) on polycrystalline $CaCO_3$ samples were performed to allow clear identification of C and O contributions in XPS. The carbonate samples were produced by pressing 5 μm powder (Alfa Aesar, 99.5%) with 200 bar thus obtaining a tablet sample.

3. Results

3.1. Adsorption of CO_2 on Ca

Fig. 2a displays the MIES spectra recorded during CO_2 exposure of a freshly prepared Ca film. The spectra are displayed offset in a waterfall manner in order to allow easy comparison of the individual spectra and tracking changes occurring during the experiment. The amount of carbon dioxide exposure is indicated by the arrow on the right hand side.

In the bottom spectrum, only one feature with a binding energy of 1.4 eV is visible. It is due to emission from metallic Ca 4s states near the Fermi level. As was the case for the adsorption of O_2 on Ca, this feature initially increases and shifts slightly towards lower binding energies. This can be understood as a consequence of the AU process as elaborated in [6].

After dosage of about 2.5 L of CO_2, a peak at a binding energy of 5.3 eV, which grows in intensity with continuing exposure, can be sensed. In accordance with our previous work [6,7,22,23], we attribute this feature to emission from O 2p states of chemisorbed oxygen on the surface.

After dosing 3 L CO_2, the spectra exhibits two additional features at binding energies of 7.8 eV and 12.3 eV, respectively. Upon further exposure to CO_2, both features grow into well resolved peaks and shift slightly towards lower binding energies of 7.6 eV and 12.1 eV, respectively. Furthermore, after dosing about 3.5 L CO_2, another peak at a binding energy of 14.3 eV appears. These three features at binding energies of 7.6 eV, 12.1 eV and 14.3 eV can be attributed to the molecular orbitals (MOs) $1a'_2$, $1e'$, $4e'$ at 7.6 eV; $3e'$, $1a'_2$ at 12.1 eV and $4a'_1$ at 14.3 eV of CO_3^{2-} [4,7,24,25]. Prolonged exposure to CO_2 leads to an increased intensity of this peak triplet, while the emission from the Ca 4s orbital is no longer detectable after dosing 10 L CO_2.

The initial step of the underlying interaction processes is well known: impinging CO_2 molecules dissociate in the vicinity of the surface and Ca–O bonds are formed. These appear as the O 2p peak. Subsequently, additional CO_2 molecules chemisorb at this surface oxygen thus forming CO_3^{2-} molecules on top of the surface [4,25]. The chemisorbed oxygen is consumed by this reaction and the O 2p feature is vanished accordingly after about 25 L of carbon dioxide exposure.

The CO_3^{2-} features at 7.8 eV and 12.3 eV are spectroscopically very similar to features induced by surface OH^- groups concerning the binding energies, however displaying a quite different peak height ratio [6]. This can prove a problem for interpretation [7], if the third feature at 14.3 eV cannot be detected precisely. We avoid this problem completely by controlling our gas exposure with QMS throughout the whole experiment: No significant amounts of water or OH can be detected this way.

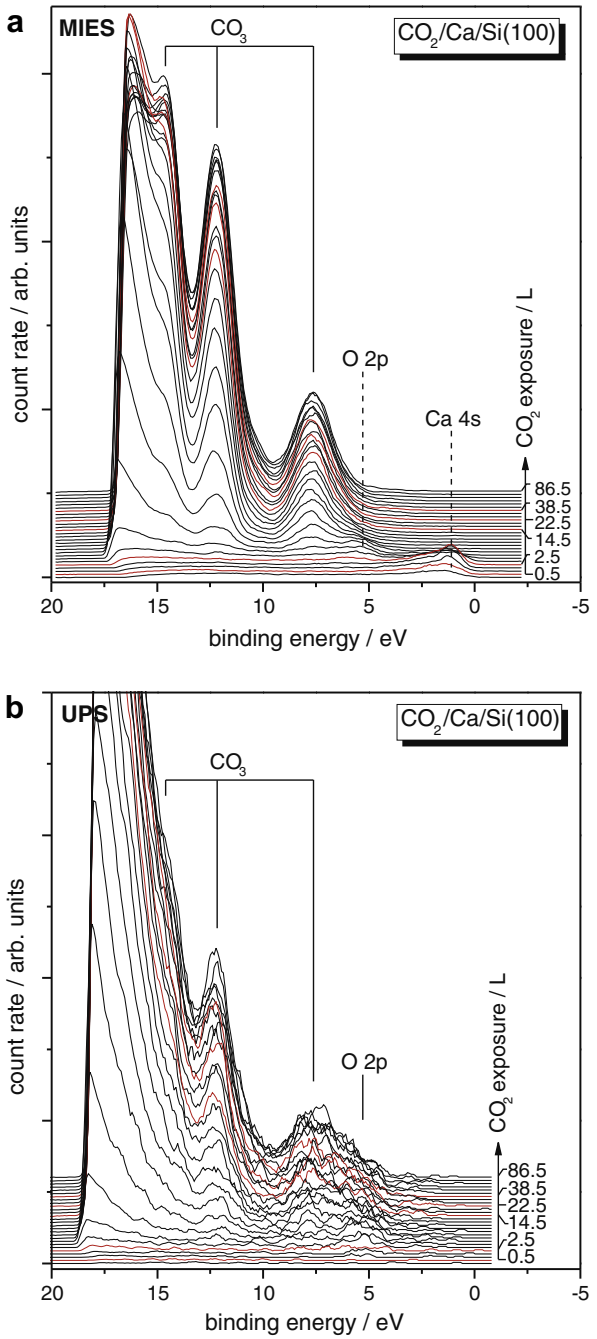

Fig. 2. MIES (a) and UPS (b) spectra of a calcium film recorded during carbon dioxide exposure.

Fig. 2b depicts the corresponding UPS spectra in the same manner as the MIES spectra discussed above. The spectrum of the clean Ca film appears structureless, which has been found before [6,7,22]. The reason for the absence of emission from Ca 4s orbitals lies in their very small cross section with UV radiation of 21.2 eV [26]. With exposure to CO_2, features at roughly the same binding energies as in the MIES spectra discussed above appear: the peak triplet which is assigned to CO_3^{2-} at binding energies of 7.7 eV, 12.1 eV and 14.3 eV, respectively, and the peak attributed to O 2p at a binding energy of 5.4 eV. In contrast to MIES, the O 2p peak does not vanish completely even at saturation, which is due to

the larger information depth of UPS. This means that the oxygen arising from the CO_2 dissociation is not completely depleted by the formation of CO_3^{2-}.

The development of the peak heights of the peaks assigned to Ca 4s, O 2p and CO_3 in MIES as well as the WF (determined by the low energy offset in the MIES spectra) as a function of CO_2 exposure is shown in Fig. 3. The oxygenation of the surface induces a WF decrease from 3.1 eV to 2.5 eV. The subsequent formation of the carbonate results in a regrowth to 2.9 eV. The O 2p feature reaches its maximum intensity around an exposure to 6 L CO_2 coinciding nearly with the work function minimum. Also at 6 L the Ca surface looses its metallic character as can be seen from the Ca 4s behaviour. It is noteworthy to realize that the CO_3 peak formation does not start until the O 2p feature is well established. The CO_3 peak triplet reaches its saturation around 30 L at the point, where the surface oxygen atoms in the outermost layer (visible as O 2p in the MIES spectra) are consumed in the CO_3^{2-} formation.

After exposure to about 30 L of carbon dioxide, the surface exhibits a complete CO_3^{2-} layer and Ca 4s or O 2p states can no longer be detected in MIES. The surface is passivated towards further CO_2 dissociation by this monolayer, and as no surface oxygen is present any longer, the generation of CO_3^{2-} comes to a standstill.

Fig. 4 shows the XPS spectra of the O 1s region (a) and the C 1s region (b) after exposure of the Ca film to 86.5 L CO_2. The points represent the original data, peak fits of the individual components are displayed using broken lines, while their sum is shown as a solid line. The O 1s peak is comprised of three contributions with binding energies of 530.9 eV, 532.3 eV and 534.3 eV, respectively. The C 1s peak is made up of two contributions with binding energies of 286.1 eV and 293.1 eV. The origins of these peaks will be discussed in Section 4.

All XPS peak fitting results including binding energies and relative contributions are summarized in Tables 1 and 2.

3.2. Adsorption of CO_2 on CaO

Fig. 5 displays the MIES (a) and UPS (b) spectra recorded during CO_2 exposure of a freshly prepared CaO film. Besides the peak of the secondary electrons MIES and UPS bottom spectra show mainly one peak at a binding energy of 5.1 eV corresponding to the ionization of O 2p orbitals in the CaO surface. The MIES spectrum of the pure CaO shows furthermore a small contamination with OH groups (peaks with binding energies of 7.1 eV and 11.7 eV in the bottom spectrum). This contamination can not be avoided [6], but is weak enough not to disturb the subsequent measurements. CaO is an insulator which is apparent from the complete absence of any contributions below binding energies of 3 eV in MIES and UPS.

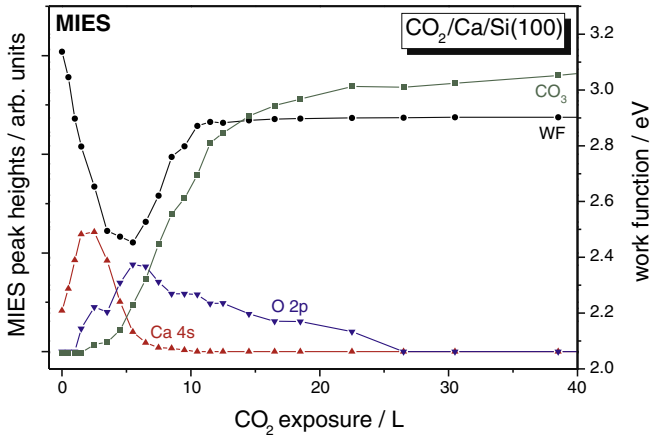

Fig. 3. MIES peak height analysis and surface work function of a calcium film plotted as a function of carbon dioxide exposure.

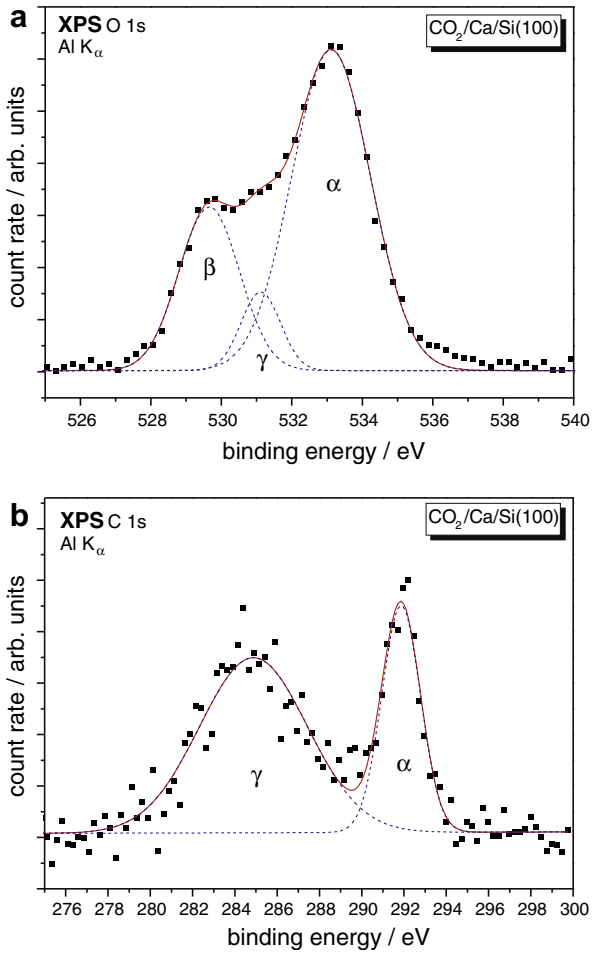

Fig. 4. XPS spectra of the O 1s (a) and C 1s (b) region of a calcium film after exposure to 86.5 L carbon dioxide.

Table 1
Summarized XPS results from the O 1s region.

System	Figure	Peak	Binding energy (eV)	FWHM (eV)	Relative intensity
CO_2/Ca	4a	β	530.9	2.0	0.26
86.5 L		γ	532.3	1.3	0.08
		α	534.3	2.6	0.66
CO_2/CaO	7a	β	530.8	1.9	0.58
81 L		α	533.5	2.8	0.42
CO/Ca	11a	β	530.3	2.4	0.34
1460 L		γ	531.7	1.0	0.04
		α	533.4	2.7	0.62
CO/CaO	14a	β	530.6	1.9	0.53
1835 L		α	533.1	2.8	0.47

Table 2
Summarized XPS results from the C 1s region.

System	Figure	Peak	Binding energy (eV)	FWHM (eV)	Relative intensity
CO_2/Ca	4b	γ	286.1	6.0	0.68
86.5 L		α	293.1	2.2	0.32
CO_2/CaO	7b	α	291.9	2.0	1
81 L					
CO/Ca	11b	γ	285.0	4.2	0.71
1460 L		α	291.7	2.1	0.29
CO/CaO	14b	α	292.0	1.8	1
1835 L					

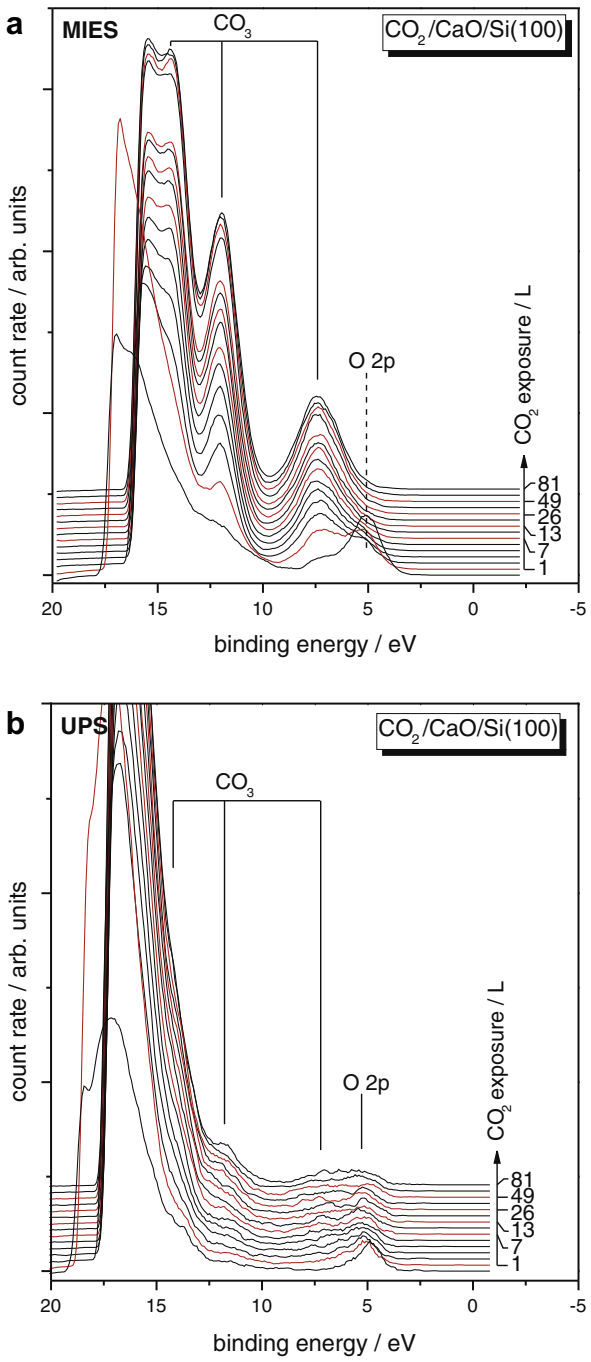

Fig. 5. MIES (a) and UPS (b) spectra of a calcium oxide film recorded during carbon dioxide exposure.

Already after a dosage of 1 L of CO_2 the carbonate peak triplet appears to be visible in the MIES spectra at binding energies 7.4 eV, 12.0 eV and 14.4 eV. Prolonged CO_2 exposure leads to an intensity increase of these peaks while O 2p, being due to the CaO surface, vanishes. The underlying process is known: impinging CO_2 molecules form CO_3^{2-} complexes with surface oxygen atoms [7,9,24]. This is very similar to the CO_3^{2-} formation on Ca films after the incorporation of oxygen from dissociated CO_2 as described in Section 3.1. Because CaO has no density of states near the Fermi level, no CO_2 dissociation is possible. Hence, no dissociation products can be detected, neither in this plot nor in the XPS results presented below. Nevertheless, CaO surfaces appear to be very reactive regarding carbonate formation.

The development of the peak heights of the peaks assigned to O 2p and CO_3 (in MIES) as well as the WF as a function of CO_2 exposure is shown in Fig. 6. The WF increases drastically and reaches its final value of about 3.4 eV at an exposure around 3 L CO_2. The intensity of emission from O 2p orbitals also decreases very quickly and reaches its minimum at about 10 L of CO_2 exposure. The CO_3^{2-} peak triplet grows very quickly to a high value around 12 L of CO_2 exposure and increases slightly afterwards. In contrast to the results for the Ca films, the CO_3^{2-} formation starts immediately with the CO_2 exposure.

Fig. 7 shows the XPS spectra of the O 1s region (a) and the C 1s region (b) after exposure of the CaO film to 81 L CO_2. The O 1s peak is comprised of two contributions with binding energies of 530.8 eV and 533.5 eV, respectively. The C 1s peak is found at a binding energy of 291.9 eV. Differently from the results for the Ca film, the peak consists of only one component. The origins of these peaks will be discussed in Section 4.

3.3. Adsorption of CO on Ca

Fig. 8 a displays the MIES spectra recorded during carbon monoxide exposure to a Ca film. Beside the emission of secondary electrons beyond binding energies of 10 eV the only feature visible in the bottom spectrum is the peak with a binding energy of 1.4 eV, which is due to emission from metallic Ca 4s states near the Fermi level as already discussed with Fig. 2. The intensity of this feature decreases and is vanished at a CO exposure of approximately 160 L. With the CO exposure again the emission from O 2p orbitals emerges at a binding energy of 5.5 eV. It grows in intensity up to a total exposure of 100 L. Prolonged CO exposure then leads to the decrease of this peak. In the top spectrum corresponding to a CO exposure of about 1460 L O 2p remains only apparent as a weak shoulder in the intense peak at a binding energy of 7.5 eV. This peak becomes visible after a CO exposure of about 50 L and grows continuously with increasing carbon monoxide exposure. At higher exposures, two more features become apparent at binding energies of 12.1 eV and 14.5 eV, respectively. As also their relative intensities of these three features match quite well with the peak triplet observed in the experiments discussed above, we identify these features as the fingerprint of CO_3^{2-}. The observed peaks are quite different from those one would expect for molecularly adsorbed CO in terms of position and shape: the features attributed to molecularly adsorbed CO are two sharp peaks at binding energies of 7.8 eV and 11.1 eV [27].

Fig. 8b displays the corresponding UPS spectra. Similar to the UPS spectrum of the pure Ca film displayed in Fig. 2b, the first

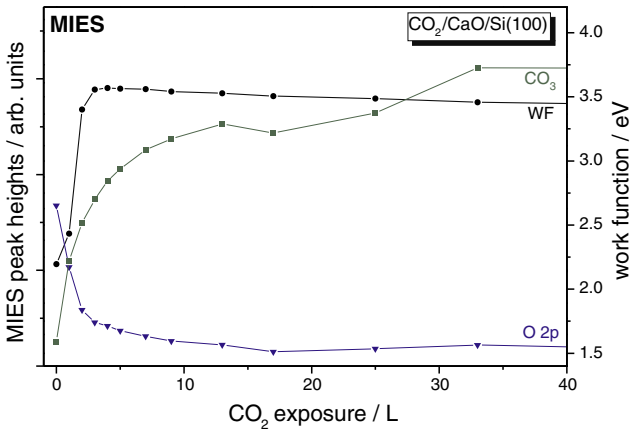

Fig. 6. MIES peak height analysis and surface work function of a calcium oxide film plotted as a function of carbon dioxide exposure.

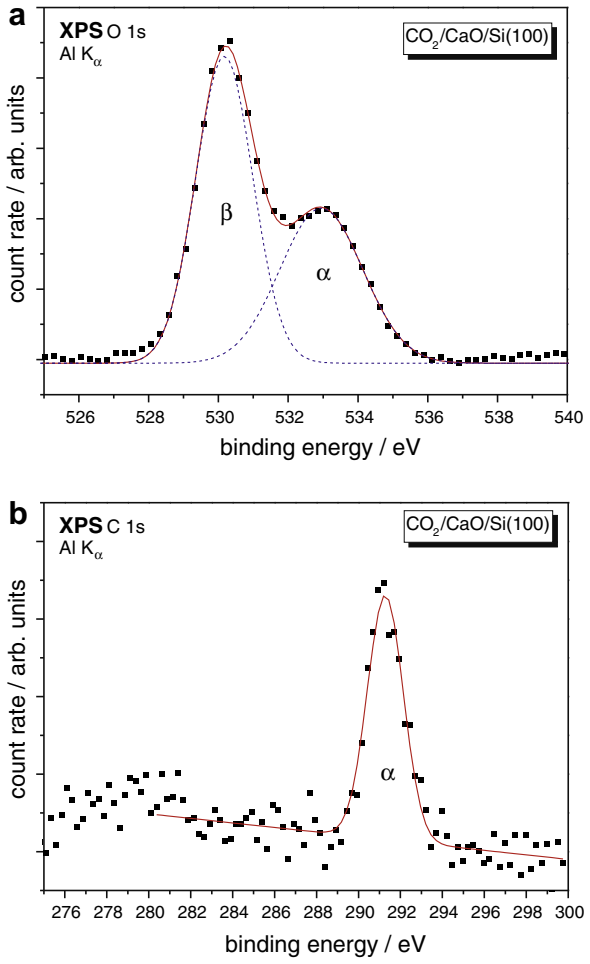

Fig. 7. XPS spectra of the O 1 s (a) and C 1s (b) region of a calcium oxide film after exposure to 81 L carbon dioxide.

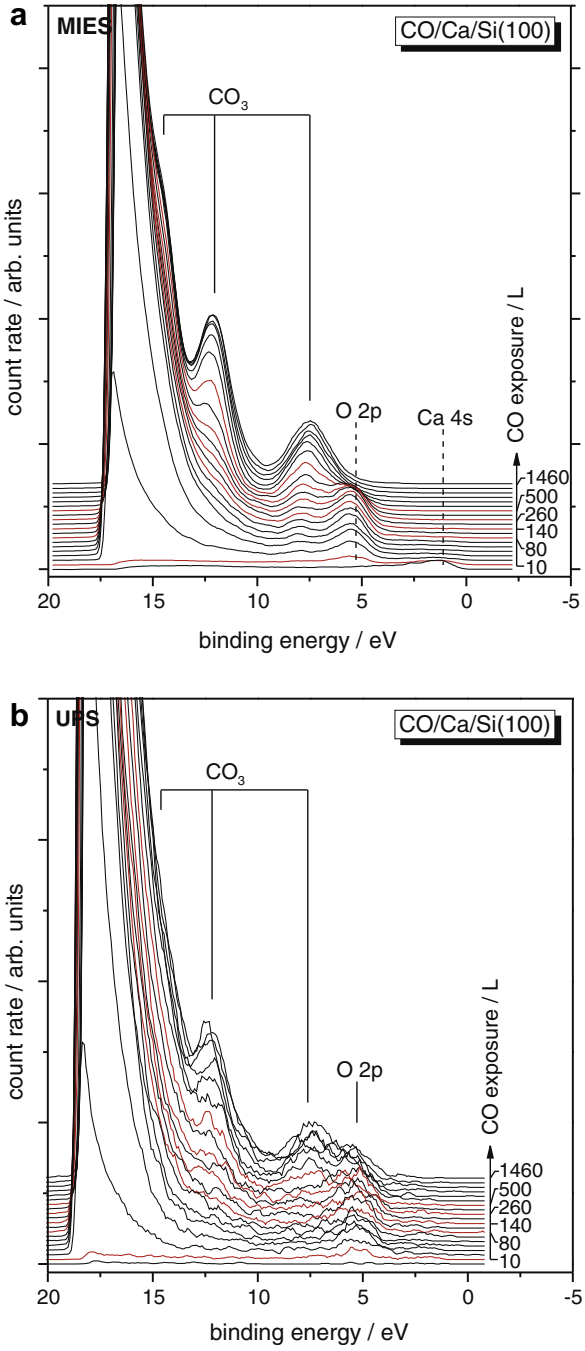

Fig. 8. MIES (a) and UPS (b) spectra of a calcium film recorded during carbon monoxide exposure.

spectrum of this series is void of significant features and appears structureless. A first peak due to O 2p emission becomes visible directly after the start of carbon monoxide exposure. The peak triplet ascribed to CO_3^{2-} develops in this series of spectra, too.

Offering CO is accompanied by a non-avoidable CO_2 contamination due to residual gas in the UHV apparatus and the gas lines, especially when dosing as high as 1460 L CO over long times. A very rigorous cleaning procedure which combines heating and evacuating cycles of the gas line is able to eliminate this contamination almost completely. Nevertheless, the continuous QMS analysis during all MIES and UPS experiments reveals that the offered CO remains contaminated by CO_2 to an amount of 0.25% integrated over the complete duration of the experiment. This means that beside the CO offer, the surfaces in Fig. 8 are exposed to at most 3.5 L CO_2.

Fig. 9 shows the top MIES spectrum of Fig. 8a, corresponding to a CO offer of 1460 L and the MIES spectrum for the Ca surface exposed to 3.5 L of CO_2 (from Fig. 2a). It is clearly visible that after an exposure of 3.5 L CO_2 large Ca 4s and O 2p emissions remain. In contrast, these features are completely vanished for the CO exposed surface, while the CO_3^{2-} fingerprint is much more pronounced. We, therefore, conclude that the observed CO_3^{2-} formation is at least mostly caused by the CO and is not only induced by CO_2 interaction with the surface. Possible mechanisms will be discussed in Section 4.

Fig. 10 shows the development of the peaks in the MIES spectra as a function of exposure. It is noticeable that the CO_3 peak is rising almost linearly with the carbon monoxide exposure but starting only after an exposure of 50 L. The O 2p feature diminishes after it reaches a maximum around 75 L CO exposure, yet it is clearly visible in the last spectrum of the sequence and thus significantly longer than it is the case in CO_2 exposure. The WF decreases initially from a starting value of 2.72 eV to a minimal value of 2.05 eV after dosage of 75 L. Subsequently it rises again – quite in accordance with the rise in intensity of the feature ascribed to CO_3^{2-} – up to a value of 2.7 eV at the end of the experiment (1460 L).

Fig. 11 shows the XPS spectra of the O 1s region (a) and the C 1s region (b) after exposure of the Ca film to 1460 L CO. The O 1s peak

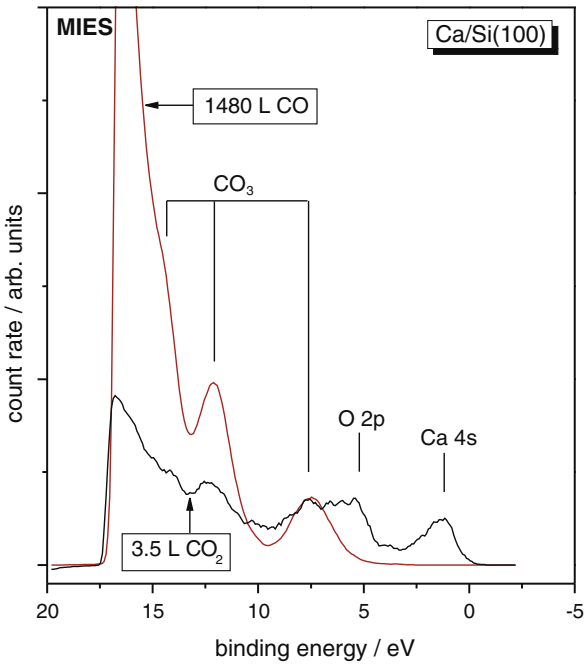

Fig. 9. The uppermost MIES spectrum from Fig. 8a and the MIES spectrum from Fig. 2a corresponding to 3.5 L carbon dioxide exposure for comparison. Count rates are not to scale.

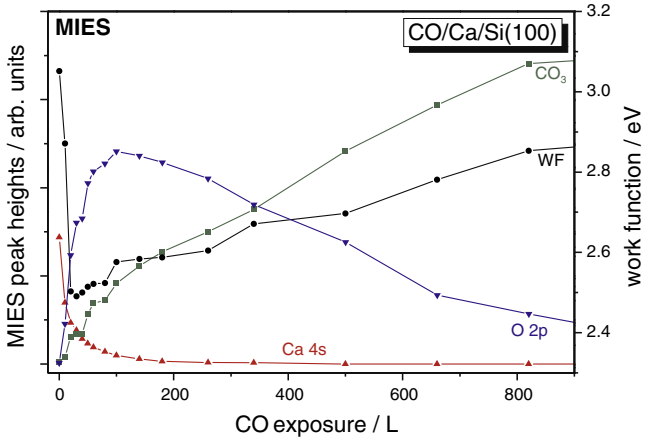

Fig. 10. MIES peak height analysis and surface work function of a calcium film plotted as a function of carbon monoxide exposure.

is comprised of three contributions with binding energies of 530.3 eV, 531.7 eV and 533.4 eV, respectively. The C 1s peak includes two contributions with binding energies of 285.0 eV and 291.7 eV. The origins of these peaks will be discussed in Section 4.

3.4. Adsorption of CO on CaO

Fig. 12 displays the MIES (a) and UPS (b) spectra recorded during CO exposure of a CaO film. The bottom spectra again mainly show the peak at a binding energy of 5.3 eV corresponding to the ionization of O 2p orbitals in the CaO surface and a small contamination with OH groups.

Already after a dosage of about 20 L of CO the well known carbonate peak triplet appears to be visible in the MIES spectra at binding energies 7.1 eV, 12.0 eV and 14.2 eV. Prolonged CO exposure leads to an intensity increase of these peaks while O 2p being due to the CaO surface vanishes almost completely. The underlying

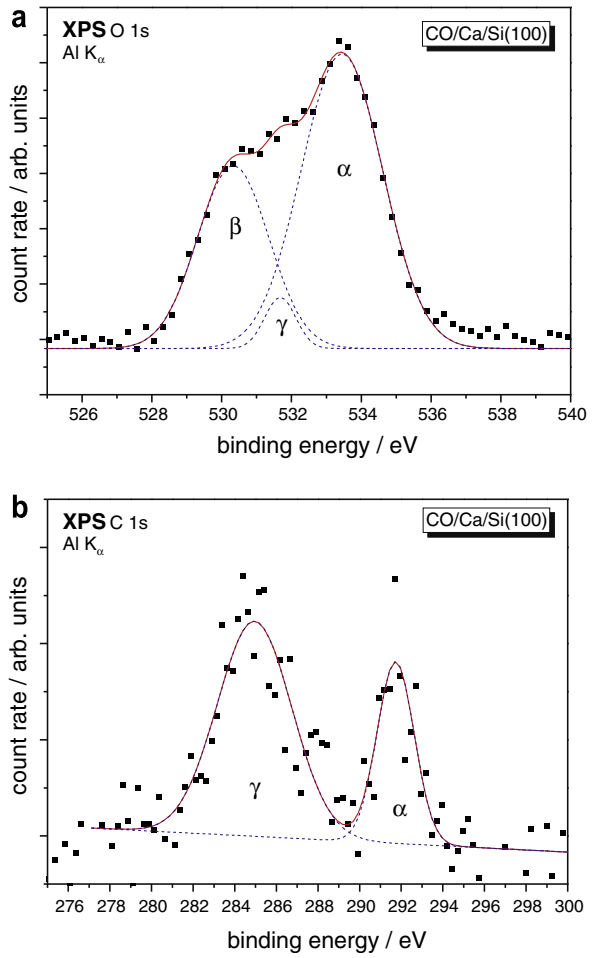

Fig. 11. XPS spectra of the O 1s (a) and C 1s (b) region of a calcium film after exposure to 1460 L carbon monoxide.

process for carbonate formation will be discussed in Section 4. The CO_3^{2-} formation is similar to the Ca films after the incorporation of oxygen from dissociated CO (as described in Section 3.1), but appears to be quicker. Because CaO is insulating no CO dissociation is possible.

The development of the peak heights of the peaks assigned to O 2p and CO_3 in MIES as well as the WF (determined by the low energy offset in the MIES spectra) as a function of CO exposure is shown in Fig. 13. The WF increases linearly and reaches its final value of about 3.5 eV at an exposure around 500 L CO. O 2p also decreases reaching its minimum value at about 700 L of CO exposure. The CO_3^{2-} formation rises very quickly to its saturation value around 150 L of CO exposure. In contrast to the results for the Ca films, the CO_3^{2-} formation starts immediately with the CO exposure.

Fig. 14 shows the XPS spectra of the O 1s region (a) and the C 1s region (b) after exposure of the CaO film to 1835 L CO. The O 1s peak is comprised of two contributions with binding energies of 530.6 eV and 533.1 eV, respectively. The one component of the C 1s peak is found at a binding energy of 292.0 eV. The origins of these peaks also will be discussed in Section 4.

4. Discussion

4.1. CO_2 adsorption

4.1.1. CaO surfaces

The formation of CO_3^{2-} complexes on top of the CaO surfaces found in this study is already known: Impinging CO_2 molecules

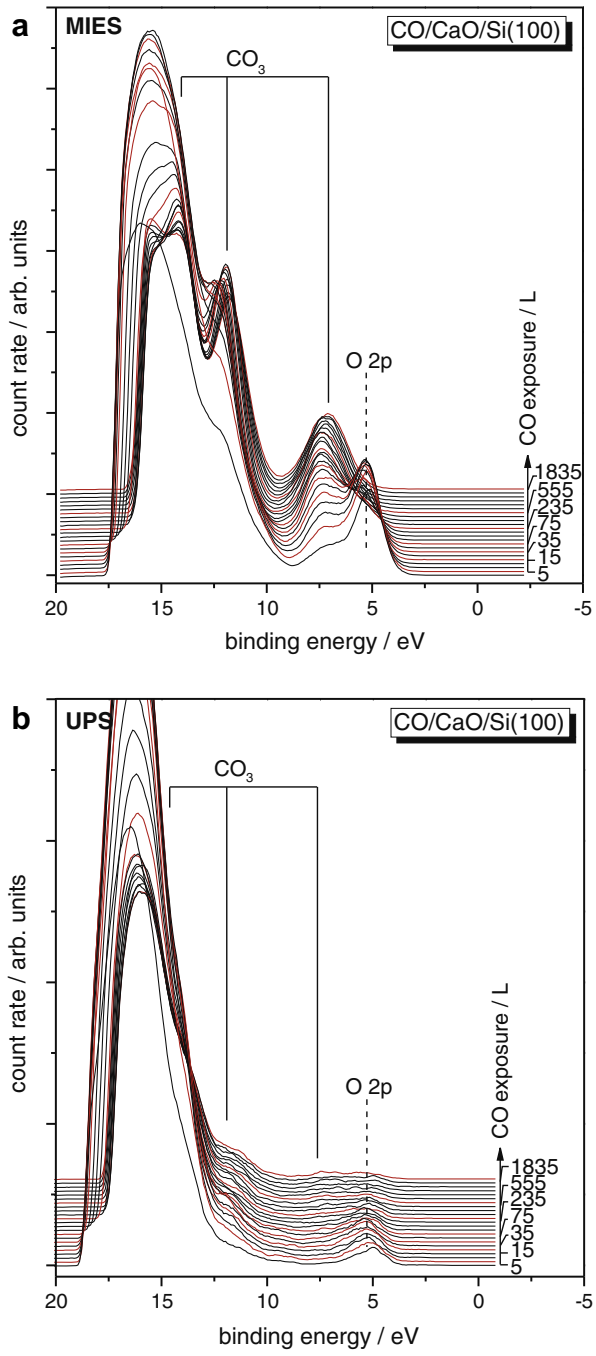

Fig. 12. MIES (a) and UPS (b) spectra of a calcium oxide film recorded during carbon monoxide exposure.

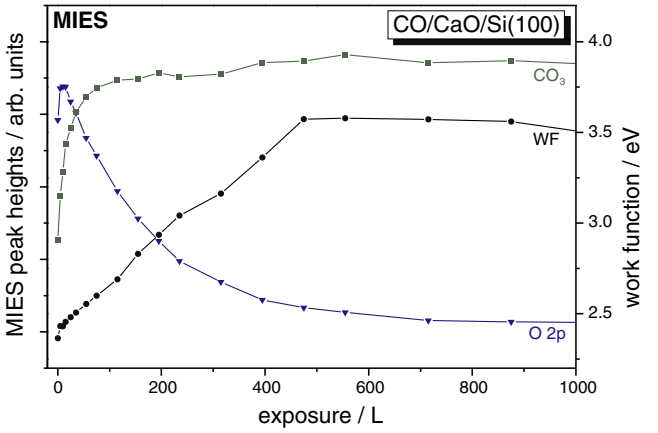

Fig. 13. MIES peak height analysis and surface work function of a calcium oxide film plotted as a function of carbon monoxide exposure.

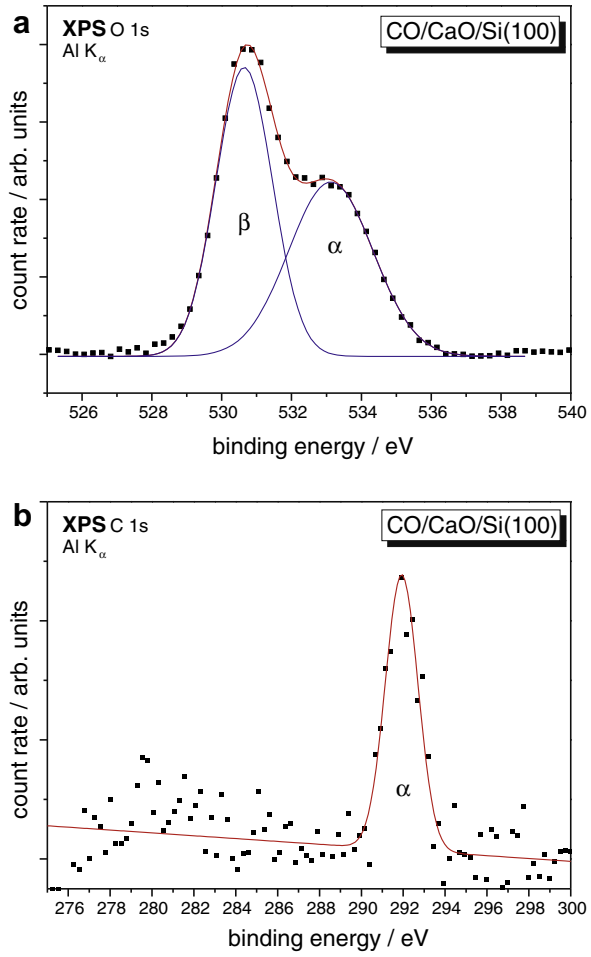

Fig. 14. XPS spectra of the O 1s (a) and C 1s (b) region of a calcium oxide film after exposure to 1835 L carbon monoxide.

are adsorbed on oxygen sites, while their O–C–O bonding angle decreases to about 130° [9]. In this way the CaO surface becomes covered with CO_3^{2-} complexes. Because no MIES signal from the underlying O 2p remains visible after saturation of the CaO surface, we assume that the surface is completely covered with CO_3^{2-} complexes, which has been observed on CaO(100) surfaces as well [9].

The carbonate formation appears to be a very fast process. The main part of the reaction is already completed at a CO_2 exposure of about 3 L, as can be deduced from the WF progress (see Fig. 6).

Because the carbonate formation is confined to the uppermost layer of the sample, the relative coverage θ ($\theta = 1$ corresponds to one complete monolayer) of the CaO surface by CO_3^{2-} complexes can be estimated by the development of the peaks denoted CO_3 in MIES (see Fig. 6). The evolution of those peaks can be fitted by a simple Langmuir isotherm

$$\frac{d\theta}{dt} = S_0 \cdot (1-\theta) \cdot \Gamma \quad (1)$$

$$\Rightarrow \theta = 1 - \exp(-S_0 \cdot \Gamma \cdot t) \quad (2)$$

where S_0 is the reaction probability for CO_2 on the uncovered CaO surface and Γ is the number of CO_2 molecules impinging per CaO unit cell and second. Using the QMS data acquired during the adsorption experiments and taking into account exposure times, the cross sections for ionization and detection in the QMS and our Penning gauge, we calculate Γ integrated over the first 3 L of CO_2 exposure to be 1.7. The reaction probability S_0 deduced from this fit amounts to about 0.6 for impinging CO_2 molecules. Similar values have been reported on ZnO(10$\bar{1}$0) [28]. This means one can estimate roughly 60% of the impinging CO_2 molecules adsorb on CaO forming a CO_3^{2-} complex. The applicability of the Langmuir isotherm confirms that the adsorption proceeds according to the simple model described above and hints at it being non-activated at room temperature. It must be stressed this is only a rough estimate using the available spectroscopic data, additional experiments with more specialised methods to confirm this finding are highly desirable. A more detailed study on CaO(100) is presented in [9].

The carbonate formation is restricted to the top surface layer, because further impinging CO_2 molecules are not able to interact with surface oxygen atoms. This is supported by the UPS results, where O 2p emission can still be detected at the end of the experiment and the features attributed to CO_3^{2-} do not grow in intensity after having reached their saturation level in the corresponding MIES spectra. Additionally, the XPS O 1s results clearly show two contributions (see Fig. 7a and Table 1): peak β due to emission from the CaO and peak α due to the emission from the CO_3^{2-}.

The XPS C 1s peak (see Fig. 7b and Table 2) shows only one component denoted α due to the emission from the CO_3^{2-} .

All XPS peak components (see Tables 1 and 2) show reasonable binding energies and FWHMs, i.e. they are consistent for all experiments and are in agreement with previous work [29] and preliminary experiments performed on CaO films (Fig. 1) and $CaCO_3$ powder (not shown here). This strongly supports our assignment of the components to carbonate or oxide, respectively. Variations are due to unavoidable charging of the surfaces, especially on CaO, and the accuracy of our setup.

The composition of the CO_3^{2-} surface layer seems to be over-stoichiometric concerning the oxygen content compared to carbon, i.e. the layer contains too much oxygen. As it is impossible to distinguish quantitatively between different chemical environments of the calcium with XPS using our setup, no information on the stoichiometry concerning calcium can be contributed.

4.1.2. Ca surfaces

On Ca surfaces carbonate formation is only possible after CO_2 dissociation in the first step. This is similar to the observations on Sr and Ba surfaces [15]. The oxygen atom from this dissociation is involved in a surface oxide formation resulting in an increase of the O 2p emission which induces a WF decrease. The WF minimum and O 2p maximum coincide at a CO_2 exposure of 6 L. CO_3^{2-} formation also sets in at the work function minimum when the amount of available O 2p atoms in the surface is sufficiently high. This results in a work function increase. We find that saturation of carbonate formation is almost completed at a CO_2 exposure of about 15 L, a value five times higher than for the saturation on CaO surfaces. Thus the reaction is significantly slower than on CaO surfaces.

The carbonate formation has been found to be very quick (see Section 4.1.1) implying that this reduced reaction rate for the complete carbonate formation process is completely dominated by the CO_2 dissociation. Basing on this we find a rate for dissociation and oxygen incorporation of about 0.1 for impinging CO_2 molecules as a rough estimate.

The carbonate formation can be verified in the XPS spectrum of the O 1s region (peak α). The additional presence of peak β gives evidence to the formation of calcium oxide under the carbonate layer. This is supported by the UPS results, where O 2p emission can be detected at the end of the experiment in contrast to MIES.

The XPS results further suggest the existence of an additional small contribution (peak γ, see Fig. 4a and Table 1) besides the peaks due to CaO (peak β) and CO_3^{2-} (peak α). This corresponds to oxygen atoms being chemisorbed but not well incorporated in an oxide or carbonate species. A similar observation has been made for the interaction of oxygen and water on Ca surfaces [6] and for CaO surfaces [29].

XPS C 1s data show interestingly the appearance of a second C emission (peak γ), which can not be explained by the CO_3^{2-} formation which has been found to be responsible for peak α. Because other sources for this peak do not exist, we conclude that C atoms from the CO_2 dissociation are incorporated into the Ca surface, indicating complete dissociation of CO_2. The amount of these C atoms is two times higher than the amount of C atoms in the CO_3^{2-}.

The O 1s to C 1s ratio is again found to be over-stoichiometric for the CO_3^{2-} layer, but corresponds well to the values found on CaO surfaces.

4.2. CO adsorption

4.2.1. CaO surfaces

The formation of CO_3^{2-} complexes on top of the CaO surfaces during CO offer is quite surprising. According to [9], the interaction between CO molecules and CaO(100) single crystal surfaces is very weak. Non-dissociative CO adsorption is found only at irregular sites, e.g. edges. These CO molecules are adsorbed via their C atoms on Ca sites. In contrast, on the polycrystalline CaO surfaces investigated here, no contributions from molecularly adsorbed CO are found in MIES or UPS spectra. These would give a clear fingerprint spectrum consisting of two peaks at binding energies of 7.8 eV ($1\pi/5\sigma$ MO) and 11.1 eV (4σ MO) [27]. We must, therefore, assume that CO adsorption does not occur to a significant amount on these surfaces. Nevertheless, the underlying process of CO_3^{2-} formation is quite unclear and will be the focus of further investigations.

Because no MIES signal from the underlying O 2p remains visible after saturation of the CaO surface, we assume that the surface is completely covered with CO_3^{2-} complexes. The integral spectral intensity of the carbonate C 1s peak is quite similar in all four cases studied here supporting the picture of the surface being completely covered.

The carbonate formation from CO exposure on CaO surfaces appears to be much slower than for CO_2 offer. Saturation is reached at an exposure of about 600 L of CO. We find that the CO_3^{2-} formation during CO exposure on CaO surfaces can also be fitted by a Langmuir isotherm, as described in Section 4.1.1 for CO_2 exposure. Making use of the QMS data acquired during the adsorption experiments, we estimate a reaction probability S_0 of roughly 0.06 for impinging CO molecules on the uncovered surface. Thus, about 6% of the CO molecules will form a CO_3^{2-} complex. The applicability of the Langmuir isotherm is a strong indication that dynamic effects like CO–CO interaction are not necessary to build carbonate complexes. Possibly, carbonate formation from CO adsorption takes place preferentially at edges or other surface defects, where several surface oxygen atoms are available. We do not know the defect density of our CaO films, but believe it to be rather high. This would account for the nearly complete coverage of the surface with CO_3^{2-} complexes that we detect with MIES.

Again, carbonate formation is restricted to the top surface layer, because further impinging CO molecules are not able to interact with surface oxygen atoms. The XPS O 1s results clearly show two contribution in this case, too (see Fig. 14a and Table 1): peak β due to emission from the CaO and peak α due to the emission from the CO_3^{2-}.

The XPS C 1s peak (see Fig. 7b and Table 2) shows only one component denoted α due to the emission from the CO_3^{2-}.

Evaluation of the peak areas in XPS yield an oxygen to carbon ratio of that is over-stoichiometric for the formed carbonate on top of the CaO surface, though not in the same degree as for CO_2 adsorption.

4.2.2. Ca surfaces

Like for the CO_2 exposure, dissociation and oxide formation are the first steps subsequently followed by carbonate formation. In contrast to CO_2 exposure, the oxide formation appears to be the quicker process meaning that the carbonate formation on the Ca–O surface is the rate limiting step. Saturation is reached at an exposure of about 850 L of CO exposure. This is equivalent to a reaction probability of roughly 0.04 for impinging CO molecules.

Alike the exposure of Ca surfaces to CO_2, the XPS spectrum of the O 1s region shows an additional small contribution (peak γ, see Fig. 11a and Table 1) besides the peaks due to CaO (peak β) and CO_3^{2-} (peak α). This is attributed again to oxygen atoms being chemisorbed but not well incorporated in oxide or carbonate.

Also like for CO_2 exposure, the XPS C 1s data show the second C emission (peak γ) due to surplus C atoms from the CO dissociation. Similar conclusions have been drawn in the case of faceted Rh(1 1 0) [30] and Pd(1 1 1) [31].

The O 1s to C 1s ratio is found to be over-stoichiometric again and is in good agreement with observations made for CO_2 adsorption.

5. Summary

Offering CO_2 to Ca films leads to the dissociation of the impinging molecules and the chemisorption of oxygen on the surface. Further CO_2 molecules will react with this surface oxygen and form a surface carbonate. After a monolayer of CO_3^{2-} has been formed, the surface is passive for further reaction. XPS then shows a surface carbonate (peak α) on top of the sample. Oxygen not involved in CO_3^{2-} formation forms calcium oxide (peak β). Surplus oxygen and carbon from the dissociation process form an unordered phase (peaks γ).

The exposure of CaO films to CO_2 results in a very fast carbonate production. Impinging CO_2 reacts with the surface oxygen and forms CO_3^{2-} complexes. After a monolayer has been formed, the reaction comes to a standstill. XPS then shows a surface carbonate (peak α) on top of the calcium oxide (peak β).

The exposure of CaO films to CO leads to the formation of a surface carbonate, too. However, the process is about two orders of magnitude slower than for CO_2. The mechanisms of this process are unknown. Nonetheless, the resulting surfaces appear to be quite similar to the ones produced with CO_2.

The same applies to CO offered to Ca films. The impinging CO is dissociated and the oxygen is chemisorbed on the calcium surface. Further CO then forms a surface carbonate. CO_2 contamination from the background is not sufficient to explain this observation. Again, the resulting surfaces are very similar to the ones produced by CO_2 exposure.

Acknowledgements

The authors gratefully acknowledge valuable technical assistance by Christiane Jana Lehmann.

References

[1] F. Solymosi, J. Mol. Catal. 65 (1991) 337.
[2] H.J. Freund, M.V. Roberts, Surf. Sci. Rep. 25 (1996) 184.
[3] W. Menesklou, H.-J. Schreiner, K.H. Härdtl, E. Ivers-Tiffée, Sens. Actuators B 59 (1999) 184.
[4] W. Maus-Friedrichs, A. Gunhold, M. Frerichs, V. Kempter, Surf. Sci. 488 (2001) 239.
[5] S. Wagner, C. Warnke, W. Menesklou, C. Argirusis, T. Damjanovic, G. Borchardt, E. Ivers-Tiffée, Solid State Ionics 177 (2006) 1607.
[6] F. Bebensee, F. Voigts, W. Maus-Friedrichs, Surf. Sci. 602 (2008) 1622.
[7] D. Ochs, B. Braun, W. Maus-Friedrichs, V. Kempter, Surf. Sci. 417 (1998) 406.
[8] Z. Hou, O. Yokata, T. Tanaka, T. Yashima, Appl. Catal. A 253 (2003) 381.
[9] E. Kadossov, U. Burghaus, J. Phys. Chem. C 112 (2008) 7390.
[10] Y. Wang, Y. Ohtsuka, J. Cat. 192 (2000) 252.
[11] C.L. Carnes, K.J. Klabunde, Chem. Mater. 14 (2002) 1806.
[12] T. Ishizuka, H. Kabashima, T. Yamaguchi, K. Tanabe, H. Hattori, Environ. Sci. Technol. 34 (2000) 2799.
[13] D. Braun, J. Heeger, Appl. Phys. Lett. 58 (1991) 1982.
[14] J. Zhu, P. Goetsch, N. Ruzycki, C.T. Campbell, J. Am. Chem. Soc. 129 (2007) 6432.
[15] M. Frerichs, F. Voigts, W. Maus-Friedrichs, Appl. Surf. Sci. 253 (2006) 950.
[16] J.H. Scofield, J. Electron Spectr. Rel. Phenom. 8 (1976) 129.
[17] National Institute of Standards and Technology Electron Inelastic-Mean-Free-Path Database 1.1, <http://www.nist.gov/srd/nist71.htm>.
[18] Y. Harada, S. Masuda, H. Ozaki, Chem. Rev. 97 (1997) 1897.
[19] H. Morgner, Adv. Atom. Mol. Opt. Phys. 42 (2000) 387.
[20] G. Ertl, J. Kuppers, Low Energy Electrons and Surface Chemistry, VCH Verlag, Weinheim, 1985.
[21] R. Hemmen, H. Conrad, Phys. Rev. Lett. 67 (1991) 1314.
[22] D. Ochs, M. Brause, B. Braun, W. Maus-Friedrichs, V. Kempter, Surf. Sci. 397 (1998) 101.
[23] D. Ochs, M. Brause, W. Maus-Friedrichs, V. Kempter, J. Electron Spectr. Rel. Phenom. 88–91 (1998) 757.
[24] Y. Fukuda, I. Toyoshima, Surf. Sci. 158 (1985) 482.
[25] S. Campbell, P. Hollins, E. McCash, M.W. Roberts, J. Electr. Spectr. Rel. Phenom. 39 (1986) 145.
[26] W.C. Price, in: C.R. Bundle, A.D. Baker (Eds.), Electron Spectroscopy: Theory, Techniques and Applications, vol. I, Academic Press, London, 1977, p. 151.
[27] M. Frerichs, F.X. Schweiger, F. Voigts, S. Rudenkiy, W. Maus-Friedrichs, V. Kempter, Surf. Int. Anal. 37 (2005) 633–640.
[28] W. Hotan, W. Göpel, R. Haul, Surf. Sci. 83 (1979) 162.
[29] P.A.W. van der Heide, J. Electr. Spectr. Rel. Phenom. 151 (2006) 79–91.
[30] F. Buatier de Mongeot, A. Toma, A. Molle, S. Lizzit, L. Petaccia, A. Baraldi, Phys. Rev. Lett. 97 (2006) 056103.
[31] G. Rupprechter, V. Kaichev, H. Unterhalt, M. Morkel, V. Bukhtiyarov, Appl. Surf. Sci. 235 (2004) 26.